Residual-based a posteriori error estimates with boundary correction for Phi-FEM

Roland Becker, Raphaël Bulle, Michel Duprez, Vanessa Lleras

Residual-based a posteriori error estimates with boundary correction for φ-FEM

Roland Becker, Raphaël Bulle*, Michel Duprez and Vanessa Lleras

February 6, 2025

Abstract

In this paper, we introduce and analyze an a posteriori error estimator for the immersed boundary finite element method called φ-FEM in the case of the Poisson-Dirichlet equation. The φ-FEM scheme used a description of the domain by a level-set function. The proposed estimator is based on the residual of the governing equations and a measure of the geometry error quantified thanks to an estimation of the level-set discretization error. We prove the global reliability of this estimator up to oscillation terms linked to the discretization of the boundary and the source term. We validate this estimator through various test cases. Its efficiency and ability to identify regions of high error and guide adaptive strategies are also investigated. Additionally, the paper compares the performance of the proposed a posteriori estimator against the standard FEM one.

1 Introduction

The finite element method (FEM) is widely used in various fields to simulate physical phenomena. For a general introduction, we refer, e.g. to [19]. Such schemes are based on a mesh, which usually coincides with the boundary of the considered domain. This constraint can be difficult to satisfy, for instance, when the domain's geometry is too complex or changes over time or during the iterations of an optimization process. In such situations, it is possible to adapt the variational formulation of the FEM to meshes which do not fit the boundary of the domain. Their variants come under the name of Immersed Boundary Methods (IBM); see, for instance, [26], for a review.

One of the first IBM [20, 21] consists of extending the solution from the actual physical domain to a larger one and imposing the boundary conditions with Lagrange multipliers or penalization terms. These methods suffer from a lack of accuracy and poor conditioning of the associated finite element matrix. A first alternative is the Finite Cell Method [27]. In the case of the elasticity equation, the authors add a soft virtual material outside the domain and an appropriate preconditioner in matrix resolution. Later on, the cutFEM approach [7, 8, 9] consists of doing integration by part of the strong formulation on the exact domain. The cells on the boundary are partially integrated, which is compensated thanks to stabilization terms like the ghost penalty [6]. More recently, in the Shifted Boundary Method (see [24]), a Taylor expansion of the boundary condition from the real boundary to the discrete one is considered.

A new IBM, called φ-FEM and introduced in [18] in the case of the Poisson-Dirichlet equation, uses a level-set function φ in the variational formulation to impose the homogeneous boundary conditions. The φ-FEM assumes that the domain Ω is described by a levelset function φ, i.e. $\Omega = \{\varphi < 0\}$ and the solution is searched in the form $u = \varphi w$ so that boundary conditions are

*Corresponding author. Inria Nancy-Grand Est (raphael.bulle@inria.fr)

automatically satisfied. The φ-FEM has optimal accuracy and a well-conditioned finite element matrix. Moreover, unlike the cutFEM paradigm, it requires no integral computation on the real boundary or some parts of the cells. The φ-FEM has been adapted to treat Neumann boundary condition [15], the Stokes [16] and heat equations [17] and also cracks and interfaces [11].

A posteriori error estimation is now a well-established tool to assess the discretization error of finite element method simulations [1, 29]. One of the main applications of a posteriori error estimators is adaptive mesh refinement [14, 25], which is essential to reduce the discretization error while keeping a tractable computational cost as soon as the solution to the problem of interest has local features such as steep gradients or singularities. The main difficulty when performing a posteriori error estimation with IBM is controlling the geometry and/or interface approximation error.

In [3], the authors derive a residual-based estimator for the IBM formulation with distributed Lagrange multipliers of a Poisson equation with a discontinuous diffusivity across an interface. The estimator takes into account the interface approximation error thanks to the difference of the finite element solutions on each side of the interface. In this context, they show the reliability and efficiency of the estimator. A reliable estimator for the Finite Cell Method (FCM) is derived in [12], applicable to *hp*-adaptive finite elements. The authors of [23] have obtained a residual-based a posteriori error estimator for a penalized immersed finite element method applied to elliptic interface problems. Their analysis demonstrated that the estimator is both reliable and efficient. This approach is generalized to the Petrov-Galerkin case in [22]. [5] introduces an advanced a posteriori error estimator based on equilibrated fluxes to assess the accuracy of numerical simulations affected by defeaturing. This term means that the geometry is simplified by removing features that are considered not relevant for the approximation of the solution of the equations. In the case of holes, this technique could be seen as a fictitious domain technique.

Despite several studies on a posteriori error estimation in the context of IBM, the literature on error estimation taking the geometry approximation into account is still sparse [2, 10, 13]. In [10], they have developed and analyzed a residual-based a posteriori error estimator for the cutFEM method. Their estimator incorporates a boundary correction which plays a key role in the reliability proof.

In the present article, we propose a residual a posteriori estimator for the φ-FEM scheme introduced in [18] in the case of Poisson equation with Dirichlet boundary conditions. In our main theoretical result (see Theorem 1), we prove the upper bound of our estimator. The originality lies in the presence of new terms representing the boundary error in the residual part and in the oscillation part.

The manuscript is organized as follows: in Section 2, we recall the φ-FEM formulation of [18]. Our residual-based error estimator is introduced in section 3 and its global reliability, which is proven in Section 5 thanks to technical tools recalled in 4. We finally give the adaptive algorithm and some numerical illustrations in Section 6.

2 Problem settings and discretizations

In our study, we consider the Poisson-Dirichlet problem

$$-\Delta u = f \quad \text{in } \Omega, \qquad u = 0 \quad \text{on } \Gamma, \tag{1}$$

where $\Omega \subset \mathbb{R}^d$ $(d = 2, 3)$ be a bounded domain with piecewise smooth boundary Γ. We assume that Ω and Γ are given by a level-set function φ such that

$$\Omega := \{\varphi < 0\} \quad \text{and} \quad \Gamma := \{\varphi = 0\}. \tag{2}$$

We assume that Ω is a subset of a simply shaped domain $\mathcal{O}$ (e.g. a box in $\mathbb{R}^d$) on which we introduce a simplicial mesh $\mathcal{T}_h^{\mathcal{O}}$ (the background mesh). We assume that $\mathcal{T}_h^{\mathcal{O}}$ is quasi-uniform,

meaning that, for any cell T, we have $\rho(T) \geqslant \beta h_T$, where h_T is the length of the longest facet of T and $\rho(T)$ the radius of the largest ball inscribed in T. For an integer $l \geqslant 1$, we consider the finite element space

$$V_{h,\mathcal{O}}^{(l)} := \left\{ v_h \in H^1(\mathcal{O}),\ v_{h|T} \in \mathbb{P}_l(T)\ \forall T \in \mathcal{T}_h^{\mathcal{O}} \right\} \tag{3}$$

and the discrete level-set $\varphi_h \in V_{h,\mathcal{O}}^{(l)}$ defined with the standard Lagrange interpolation operator $I_{h,\mathcal{O}}^{(l)}$ on $V_{h,\mathcal{O}}^{(l)}$:

$$\varphi_h := I_{h,\mathcal{O}}^{(l)}(\varphi). \tag{4}$$

Therefore the smooth boundary $\Gamma = \{\varphi = 0\}$ is approached by the piecewise polynomial boundary $\Gamma_h = \{\varphi_h = 0\}$. The discrete level-set φ_h is employed in the numerical scheme to simplify its implementation.

Let $\mathcal{T}_h$ be a submesh of $\mathcal{T}_h^{\mathcal{O}}$ composed of the elements having a non-empty intersection with the discrete domain $\{\varphi_h < 0\}$. We denote by Ω_h the domain occupied by $\mathcal{T}_h$, in other words,

$$\mathcal{T}_h := \left\{ T \in \mathcal{T}_h^{\mathcal{O}};\ T \cap \{\varphi_h < 0\} \neq \varnothing \right\} \quad \text{and} \quad \Omega_h := \left(\cup_{T \in \mathcal{T}_h} T\right)^{\circ}. \tag{5}$$

We denote by $\mathcal{F}_h$ the set composed by the facets of the cells belonging to $\mathcal{T}_h$. Take the integer $k \geqslant 1$ and consider the finite element space

$$V_h^{(k)} := \left\{ v_h \in H^1(\Omega_h);\ v_{h|T} \in \mathbb{P}_k(T)\ \forall T \in \mathcal{T}_h \right\}. \tag{6}$$

We recall the φ-FEM approximation to eq. (1) introduced in [18]: find $w_h \in V_h^{(k)}$ such that

$$a_h(w_h, v_h) = l_h(v_h) \quad \forall v_h \in V_h^{(k)}, \tag{7}$$

where, for all $w_h, v_h \in V_h^{(k)}$, the bilinear form a_h and linear form l_h are defined by

$$a_h(w_h, v_h) := \int_{\Omega_h} \nabla(\varphi_h w_h) \cdot \nabla(\varphi_h v_h) - \int_{\partial\Omega_h} \frac{\partial}{\partial n}(\varphi_h w_h)\varphi_h v_h + G_h(w_h, v_h) \tag{8}$$

and

$$l_h(v_h) := \int_{\Omega_h} f_h \varphi_h v_h + G_h^{\mathrm{rhs}}(v_h), \tag{9}$$

with $f_h = \Pi_h f$ the L^2 projection of f on $V_h^{(k)}$ and G_h, G_h^{rhs} standing for

$$G_h(w_h, v_h) := \sigma \sum_{E \in \mathcal{F}_h^{\Gamma}} h_E \int_E \left[\frac{\partial}{\partial n}(\varphi_h w_h)\right]\left[\frac{\partial}{\partial n}(\varphi_h v_h)\right] + \sigma \sum_{T \in \mathcal{T}_h^{\Gamma}} h_T^2 \int_T \Delta(\varphi_h w_h)\Delta(\varphi_h v_h), \tag{10}$$

and

$$G_h^{\mathrm{rhs}}(v_h) := -\sigma \sum_{T \in \mathcal{T}_h^{\Gamma}} h_T^2 \int_T f \Delta(\varphi_h v_h). \tag{11}$$

Here $\sigma > 0$ is a stabilization parameter, $\mathcal{T}_h^{\Gamma} \subset \mathcal{T}_h$ is composed of the cells cut by the discrete boundary $\Gamma_h = \{\varphi_h = 0\}$, i.e.

$$\mathcal{T}_h^{\Gamma} := \{T \in \mathcal{T}_h;\ T \cap \Gamma_h \neq \varnothing\},\ \Omega_h^{\Gamma} := \left(\cup_{T \in \mathcal{T}_h^{\Gamma}} T\right)^{\circ}, \tag{12}$$

and $\mathcal{F}_h^{\Gamma}$ is the set of internal facets of the mesh $\mathcal{T}_h$ belonging to a cut cell

$$\mathcal{F}_h^{\Gamma} := \{F \text{ an internal facet of } \mathcal{T}_h \text{ such that } \exists\ T \in \mathcal{T}_h;\ T \cap \Gamma_h \neq \varnothing \text{ and } F \in \partial T\}. \tag{13}$$

We also denote by $\mathcal{F}_h^I$ and $\mathcal{F}_h^B$ the sets of internal and boundary facets of $\mathcal{T}_h$ respectively. Given a function $v \in H^1(\Omega_h)$ and an facet $E \in \mathcal{F}_h^I$ we will use the notation $[v]_E$ (or simply $[v]$ when there is no ambiguity) for the jump of v across the facet E.

3 Main results : global reliability

In this section, we introduce our residual-based a posteriori error estimate for the H^1 semi-norm and state the main results, namely, its global reliability.

Let f_h be the L^2 projection of f in $V_h^{(k)}$. For a cell $T \in \mathcal{T}_h$ and an facet $E \in \mathcal{F}_h^I$, we denote

$$r_T := (f_h + \Delta u_h)_T \quad \text{and} \quad J_E := \left[\frac{\partial}{\partial n} u_h\right]_E . \tag{14}$$

Introduce the boundary correction function

$$\varepsilon_h = (\varphi_h - \varphi_{h,\text{fine}}) w_h,$$

where $\varphi_{h,\text{fine}}$ is the standard Lagrange interpolation of φ on $V_{h,\text{fine}}^{(k)}$, with $V_{h,\text{fine}}^{(k)}$ defined as follows: consider $\mathcal{T}_{h,\text{fine}}$ the mesh $\mathcal{T}_h$ in which we have refined the cell of $\mathcal{T}_h^\Gamma$ and associated finite element space

$$V_{h,\text{fine}}^{(k)} = \left\{ v_h \in H^1(\Omega_h);\ v_{h|T} \in \mathbb{P}_k(T)\ \forall T \in \mathcal{T}_{h,\text{fine}} \right\}.$$

For a cell $T \in \mathcal{T}_h$ the local contribution of the residual H^1 semi-norm error estimator is given by

$$\eta_T^2 := \eta_{r,T}^2 + \eta_{J,T}^2 + \eta_{\varepsilon,T}^2, \tag{15}$$

where

$$\eta_{r,T} := h_T \|r_T\|_T, \quad \eta_{J,T} := \frac{1}{2} \left[\sum_{E \in \partial T} h_E \|J_E\|_E^2 \right]^{1/2}, \quad \eta_{\varepsilon,T} := |\varepsilon_h|_{1,T} \tag{16}$$

and the global estimator by

$$\eta^2 = \eta_r^2 + \eta_J^2 + \eta_\varepsilon^2 = \sum_{T \in \mathcal{T}_h} \left(\eta_{r,T}^2 + \eta_{J,T}^2 + \eta_{\varepsilon,T}^2 \right). \tag{17}$$

The quantities $\eta_{r,T}$, $\eta_{J,T}$ and $\eta_{\varepsilon,T}$ will be respectively called the interior residual, the facet residual and the boundary correction term.

Let us now state our main result, the global reliability of our estimator:

Theorem 1. *Suppose that $\Omega \subset \Omega_h$. Let u and u_h be the solutions to Systems (1) and (7), respectively. We have*

$$|u - u_h|_{1,\Omega}^2 \leqslant C(\eta^2 + \text{osc.}^2), \tag{18}$$

where

$$\text{osc.}^2 = \sum_{T \in \mathcal{T}_h} h_T^2 \|f - f_h\|_{0,T}^2 + |\xi - \varepsilon_h|_{1,\Omega_h}^2$$

and $\xi = u_h - \Pi(u_h)$, with $\Pi(u_h)$ is the projection of u_h in $H_0^1(\Omega)$, i.e the solution of

$$\int_\Omega \nabla(\Pi(u_h)) \cdot \nabla v = \int_\Omega \nabla u_h \cdot \nabla v, \quad \forall v \in H_0^1(\Omega). \tag{19}$$

In eq. (15), $\eta_{\varepsilon,T}$ is the only non-standard contribution. Therefore, let us emphasize a few comments about it:

- In the expression of ε_h, the term $\varphi_h - \varphi_{h,\text{fine}}$ measures the boundary error which is weighted by w_h. Thus, ε_h can be seen as an estimator of the boundary condition error in u_h and therefore, as the boundary approximation error since we consider homogeneous zero Dirichlet boundary condition.

- Let us give a justification for the choice of $\eta_{\varepsilon,T}$. As we will see in the proof of Theorem 1, an optimal choice would have been ξ, but this quantity needs the resolution of eq. (19) which is defined on the (unknown) exact domain Ω. One could resort to a numerical resolution of eq. (19) in e.g. a finer finite element space. However, this would lead to a prohibitive computational cost. Thus, we choose instead to bound the norm of ξ by the quantity η_ε (up to negligible terms) which is has the advantage to be cheap to compute. Indeed, since only the cells of $\mathcal{T}_h^\Gamma$ have been refined in $\mathcal{T}_h$ for the construction of $\mathcal{T}_{h,\text{fine}}$, we remark that

$$\begin{aligned}
|\xi|^2_{1,\Omega_h} = |u_h - \Pi(u_h)|^2_{1,\Omega_h} &= \inf_{z\in H^1_0(\Omega)} |u_h - z|^2_{1,\Omega_h} \\
&\leqslant |(\varphi_h - \varphi) w_h|^2_{1,\Omega_h} \\
&\leqslant 2|(\varphi_h - \varphi_{h,\text{fine}}) w_h|^2_{1,\Omega_h^\Gamma} + 2|(\varphi_{h,\text{fine}} - \varphi) w_h|^2_{1,\Omega_h^\Gamma} \\
&\leqslant C \left(\sum_{T\in\mathcal{T}_h^\Gamma} \eta^2_{\varepsilon,T} + \sum_{T\in\mathcal{T}_{h,\text{fine}}\cap\Omega_h^\Gamma} h_T^2 |\varphi|^2_{2,T} \|w_h\|^2_{W^1_\infty(T)} \right),
\end{aligned}$$

  thanks to classical interpolation inequalities.

- Moreover, the norm of ξ will be smaller than the error in the H^1 semi-norm:

$$|\xi|_{1,\Omega_h} = \inf_{z\in H^1_0(\Omega)} |u_h - z|_{1,\Omega_h} \leqslant |u_h - u|_{1,\Omega_h}.$$

4 Assumptions on the mesh and technical tools

The two following assumptions on the levelset φ and the mesh $\mathcal{T}_h$ are needed in [18] for the convergence of the scheme (7):

Assumption 1. *The boundary Γ can be covered by open sets $\mathcal{O}_i$ for $i = 1,\dots,I$ and one can introduce on every $\mathcal{O}_i$ local coordinates $\xi_1,\dots,\xi_d$ with $\xi_d = \varphi$ such that all the partial derivatives $\partial^\alpha \xi/\partial x^\alpha$ and $\partial^\alpha x/\partial \xi^\alpha$ up to order $k+1$ are bounded by some $C_0 > 0$. Moreover, $|\varphi| \geqslant m$ on $\mathcal{O} \setminus \cup_{i=1,\dots,I}\mathcal{O}_i$ with some $m > 0$.*

Assumption 2. *The approximate boundary Γ_h can be covered by element patches $\{\Pi_i\}_{i=1,\dots,N_\Pi}$ having the following properties:*

- *Each patch Π_i is a connected set composed of a mesh element $T_i \in \mathcal{T}_h \setminus \mathcal{T}_h^\Gamma$ and some mesh elements cut by Γ_h. More precisely, $\Pi_i = T_i \cup \Pi_i^\Gamma$ with $\Pi_i^\Gamma \subset \mathcal{T}_h^\Gamma$ containing at most M mesh elements;*
- *$\mathcal{T}_h^\Gamma = \cup_{i=1}^{N_\Pi} \Pi_i^\Gamma$;*
- *Π_i and Π_j are disjoint if $i \neq j$.*

The Lemma below proven in [18] is a generalization of the Hardy inequality:

Lemma 1. *We assume that the domain Ω is given by the level-set φ, cf. (2), and satisfies Assumption 1. Then, for any $u \in H^{k+1}(\mathcal{O})$ vanishing on Γ,*

$$\left\| \frac{u}{\varphi} \right\|_{k,\mathcal{O}} \leq C \|u\|_{k+1,\mathcal{O}}$$

with $C > 0$ depending only on the constants in Assumption 1.

We introduce an extended band of mesh elements near the boundary Γ, namely the submesh $\mathcal{T}_h^{\Gamma,ext}$ with $\mathcal{T}_h^{\Gamma} \subset \mathcal{T}_h^{\Gamma,ext} \subset \mathcal{T}_h$ by adding to $\mathcal{T}_h^{\Gamma}$ the cells which are neighbors and neighbors of neighbors of cells in $\mathcal{T}_h^{\Gamma}$. We suppose that:

Assumption 3. *$|\nabla\varphi| \geqslant m$, $|\nabla\varphi_h| \geqslant \frac{m}{2}$ on all the mesh cells in $\mathcal{T}_h^{\Gamma,ext}$, $|\varphi| \geqslant mh$ on $\mathcal{T}_h \setminus \mathcal{T}_h^{\Gamma,ext}$, and $|\nabla\varphi_h| \leqslant M$ on Ω_h with some $m, M > 0$.*

The following Lemma can be proven by adapting the proof of [16, Lemma 6]:

Lemma 2. *For any $v \in H_0^1(\Omega_h)$, there exists $z_h \in V_h^{(k)}$ s.t. for all cells $T \in \mathcal{T}_h$*

$$\|v - \varphi_h z_h\|_{0,T} \leqslant Ch_T(|v|_{1,\omega_T} + \|w\|_{0,\omega_T}),$$

where, $w = v/\varphi$, ω_T is the union of cells shared a node with T and $C > 0$ depending only on the constants in Assumptions 1 and 3, and the mesh regularity.

5 Proof of Theorem 1

Let us denote by $e = u_h - u$. Consider $\Pi(u_h)$ projection of u_h in $H_0^1(\Omega)$, in other words for all $v \in H_0^1(\Omega)$ we have

$$\int_\Omega \nabla(\Pi(u_h)) \cdot \nabla v = \int_\Omega \nabla u_h \cdot \nabla v. \tag{20}$$

Thus, since $\Pi(u_h) - u_h \in H_0^1(\Omega)$ and since $\Pi(u_h) - u$ is orthogonal to $H_0^1(\Omega)$, we have

$$|e|_{1,\Omega}^2 = |\Pi(u_h) - u|_{1,\Omega}^2 + |u_h - \Pi(u_h)|_{1,\Omega}^2 = |\Pi(u_h) - u|_{1,\Omega}^2 + |\xi|_{1,\Omega}^2. \tag{21}$$

Again, since $\Pi(u_h) - u_h \in H_0^1(\Omega)$,

$$|\Pi(u_h) - u_h|_{1,\Omega} = \sup_{\substack{v \in H_0^1(\Omega) \\ |v|_{1,\Omega} \neq 0}} \frac{\langle \nabla(\Pi(u_h) - u_h), \nabla v\rangle_\Omega}{|v|_{1,\Omega}}.$$

Let $v \in H_0^1(\Omega)$ and consider $\widetilde{v}$ a Stein extension of $v \in H_0^1(\Omega)$ (see e.g. [28]) such that

$$|\widetilde{v}|_{1,\Omega_h} \leqslant C|v|_{1,\Omega}. \tag{22}$$

Since $\widetilde{v} \in H_0^1(\Omega)$, if we take $\widetilde{w} = \widetilde{v}/\varphi$, then, using Lemma 2, there exists $z_h \in V_h^{(k)}$ such that for all cell $T \in \mathcal{T}_h$

$$\|\widetilde{v} - \varphi_h z_h\|_{0,T} \leqslant Ch_T(|\widetilde{v}|_{1,\omega_T} + \|\widetilde{w}\|_{0,\omega_T}). \tag{23}$$

For $v_h = \varphi_h z_h$, using eqs. (19) and (22) one has

$$\begin{aligned}
\langle \nabla(\Pi(u_h) - u), \nabla v\rangle_\Omega &= -\int_\Omega \nabla u \cdot \nabla v + \int_\Omega \nabla\Pi(u_h) \cdot \nabla v \\
&= -\int_\Omega \nabla u \cdot \nabla v + \int_\Omega \nabla u_h \cdot \nabla v \\
&= -\int_\Omega fv + \int_{\Omega_h} \nabla u_h \cdot \nabla\widetilde{v} - \int_{\Omega_h \setminus \Omega} \nabla u_h \cdot \nabla\widetilde{v} \\
&= \underbrace{-\int_\Omega fv}_{\text{(I)}} + \underbrace{\int_{\Omega_h} \nabla u_h \cdot \nabla v_h}_{\text{(II)}} + \underbrace{\int_{\Omega_h} \nabla u_h \cdot \nabla(\widetilde{v} - v_h)}_{\text{(III)}} \underbrace{- \int_{\Omega_h \setminus \Omega} \nabla u_h \cdot \nabla\widetilde{v}}_{\text{(IV)}}.
\end{aligned}$$

Let us analyze each term in the right hand side:

$$(\mathrm{I}) = -\int_{\Omega_h} f_h \widetilde{v} + \int_{\Omega_h \setminus \Omega} f_h \widetilde{v} - \int_{\Omega} (f - f_h) v.$$

Since $v_h = \varphi_h z_h$ with $z_h \in V_h^{(k)}$, using the discrete formulation (7),

$$(\mathrm{II}) = \int_{\partial\Omega_h} \nabla u_h \cdot n v_h + \int_{\Omega_h} f_h v_h - G(u_h, v_h) + G_{\mathrm{rhs}}(v_h).$$

Thanks to an integration by parts,

$$\begin{aligned}(\mathrm{III}) &= -\sum_{T\in\mathcal{T}_h} \int_T \Delta u_h (\widetilde{v} - v_h) + \sum_{F\in\mathcal{F}_h} \int_F \nabla u_h \cdot n (\widetilde{v} - v_h) \\ &= -\sum_{T\in\mathcal{T}_h} \int_T \Delta u_h (\widetilde{v} - v_h) + \frac{1}{2} \sum_{F\in\mathcal{F}_h^I} \int_F [\nabla u_h \cdot n] (\widetilde{v} - v_h) + \int_{\partial\Omega_h} \nabla u_h \cdot n (\widetilde{v} - v_h)\end{aligned}$$

and, since $\widetilde{v} = 0$ on $\partial\Omega$,

$$\begin{aligned}(\mathrm{IV}) &= \sum_{T\in\mathcal{T}_h} \int_{T\setminus\Omega} \Delta u_h \widetilde{v} - \sum_{F\in\mathcal{F}_h} \int_{F\cap(\Omega_h\setminus\Omega)} \nabla u_h \cdot n \widetilde{v} \\ &= \sum_{T\in\mathcal{T}_h} \int_{T\setminus\Omega} \Delta u_h \widetilde{v} - \frac{1}{2} \sum_{F\in\mathcal{F}_h^I} \int_{F\cap(\Omega_h\setminus\Omega)} [\nabla u_h \cdot n] \widetilde{v} - \int_{\partial\Omega_h} \nabla u_h \cdot n \widetilde{v}.\end{aligned}$$

We remark that in (II)-(IV), the sum of the boundary terms is equal to zero. We deduce that

$$\begin{aligned}\langle \nabla(\Pi(u_h) - u), \nabla v\rangle_\Omega = &\underbrace{-\sum_{T\in\mathcal{T}_h} \int_T (\Delta u_h + f_h)(\widetilde{v} - v_h)}_{(\mathrm{A})} \underbrace{+\frac{1}{2} \sum_{F\in\mathcal{F}_h^I} \int_F [\nabla u_h \cdot n] (\widetilde{v} - v_h)}_{(\mathrm{B})} \\ &\underbrace{+\sum_{T\in\mathcal{T}_h} \int_{T\setminus\Omega} (\Delta u_h + f_h)\widetilde{v}}_{(\mathrm{C})} \underbrace{-\frac{1}{2} \sum_{F\in\mathcal{F}_h^I} \int_{F\cap(\Omega_h\setminus\Omega)} [\nabla u_h \cdot n] \widetilde{v}}_{(\mathrm{D})} \underbrace{-G(u_h, v_h) + G_{\mathrm{rhs}}(v_h)}_{(\mathrm{E})} \underbrace{-\int_\Omega (f - f_h)\widetilde{v}}_{(\mathrm{F})}.\end{aligned}$$

Let us estimate each term in the right hand side. By the Cauchy–Schwarz inequality, inequality (23), Lemma 1 and (22)

$$\begin{aligned}(\mathrm{A}) &\leqslant \sum_{T\in\mathcal{T}_h} \|\Delta u_h + f_h\|_{0,T} \|\widetilde{v} - v_h\|_{0,T} \\ &\leqslant \sum_{T\in\mathcal{T}_h} h_T \|\Delta u_h + f_h\|_{0,T} (|\widetilde{v}|_{1,\omega_T} + \|\widetilde{w}\|_{0,\omega_T}) \\ &\leqslant \left(\sum_{T\in\mathcal{T}_h} h_T^2 \|\Delta u_h + f_h\|_{0,T}^2 \right)^{1/2} (|\widetilde{v}|_{1,\Omega_h} + \|\widetilde{w}\|_{0,\Omega_h}) \\ &\leqslant C \left(\sum_{T\in\mathcal{T}_h} h_T^2 \|\Delta u_h + f_h\|_{0,T}^2 \right)^{1/2} |v|_{1,\Omega}.\end{aligned}$$

Similarly, using the trace inequality,

$$(\mathrm{B}) \leqslant C \left(\sum_{T \in \mathcal{T}_h} \frac{1}{2} \sum_{E \in \partial T \cap \mathcal{F}_h^I} h_E \|J_E\|_E^2 \right)^{1/2} |v|_{1,\Omega}.$$

For each $T \in \mathcal{T}_h^\Gamma$, since T is to a distance of order h_T to Γ, there exists a patch $\widetilde{\omega}_T$ (union of connected cells containing T) of size Ch_T intersecting Γ. By the Poincaré and discrete Cauchy–Schwarz inequalities

$$\begin{aligned}(\mathrm{C}) &\leqslant \sum_{T \in \mathcal{T}_h^\Gamma} \|\Delta u_h + f_h\|_{0,T} \|\widetilde{v}\|_{0,\widetilde{\omega}_T} \leqslant C \sum_{T \in \mathcal{T}_h^\Gamma} h_T \|\Delta u_h + f_h\|_{0,T} |\widetilde{v}|_{1,\widetilde{\omega}_T} \\ &\leqslant C \left(\sum_{T \in \mathcal{T}_h} h_T^2 \|\Delta u_h + f_h\|_{0,T}^2 \right)^{1/2} |v|_{1,\Omega}.\end{aligned}$$

Similarly, using the trace inequality,

$$(\mathrm{D}) \leqslant C \left(\sum_{T \in \mathcal{T}_h^\Gamma} \frac{1}{2} \sum_{E \in \partial T \cap \mathcal{F}_h^I} h_E \|J_E\|_E^2 \right)^{1/2} |v|_{1,\Omega}.$$

Let us estimate now term (E). By definition of G and G_{rhs},

$$(\mathrm{E}) = \underbrace{-\sigma \sum_{T \in \mathcal{T}_h^\Gamma} h_T^2 \int_T (\Delta u_h + f_h) \Delta v_h}_{(E_1)} \underbrace{-\sigma \sum_{E \in \mathcal{F}_h^\Gamma} h_E \int_E \left[\frac{\partial}{\partial n} u_h \right] \left[\frac{\partial}{\partial n} v_h \right]}_{(E_2)}.$$

Using the inverse inequality and the discrete Cauchy–Schwarz inequality

$$(E_1) \leqslant C \sum_{T \in \mathcal{T}_h^\Gamma} h_T \|\Delta u_h + f_h\|_{0,T} |v_h|_{1,T} \leqslant C \left(\sum_{T \in \mathcal{T}_h^\Gamma} h_T^2 \|\Delta u_h + f_h\|_{0,T}^2 \right)^{1/2} |v_h|_{1,\Omega_h}.$$

Moreover, by the triangle inequality, (23) and the Poincaré inequality, one has

$$|v_h|_{1,\Omega_h} \leqslant |\widetilde{v} - v_h|_{1,\Omega_h} + |\widetilde{v}|_{1,\Omega_h} \leqslant C |v|_{1,\Omega}.$$

Using the trace inequality, the second part (E_2) can be treated similarly. Finally, since $f_h = \Pi_h f$ is the L^2 projection of f in $V_h^{(k)}$, denoting by $\Pi_h v$ the L^2 projection of $\widetilde{v}$ in $V_h^{(k)}$, we deduce that

$$\begin{aligned}(\mathrm{F}) = -\int_\Omega (f - f_h)(v - \Pi_h v) &\leqslant C \sum_{T \in \mathcal{T}_h} h_T \|f - f_h\|_{0,T} |\widetilde{v}|_{1,T} \\ &\leqslant C \left(\sum_{T \in \mathcal{T}_h} h_T^2 \|f - f_h\|_{0,T}^2 \right)^{1/2} |v|_{1,\Omega}.\end{aligned}$$

Which concludes the proof.

6 Numerical results

For the simulation presented in this section, we use the `python` library `FEniCSx` (see [4]). All the codes are freely available on

`https://github.com/PhiFEM/residual-a-posteriori-error-estimate`

In all the test cases, we take $l = k = 1$ (in other words, w_h and φ_h are both piecewise linear functions) and $\varphi_{h,\text{fine}}$ as a piecewise quadratic interpolation of φ. When exact errors are provided, they have been approached by comparing the solution u_h to a reference solution u_{ref}. This reference solution is defined either as an interpolation of an analytical solution or, when there is no analytical solution, as a finer FEM approximation on a conforming mesh. The exact error computations are carried out in a Lagrange space of higher degree (typically $k+1$) defined on a finer *conforming* mesh, using the non-matching meshes interpolation routine from `FEniCSx`. When needed (for the sake of comparison with the residual estimator), the exact errors are interpolated back to the φ-FEM original mesh (such as on fig. 8).

Our adaptive mesh refinement algorithm consists of the following feedback loop

$$\cdots \longrightarrow \text{SOLVE} \longrightarrow \text{ESTIMATE} \longrightarrow \text{MARK} \longrightarrow \text{REFINE} \longrightarrow \cdots \tag{24}$$

Here is a brief description of each module.

- The SOLVE module consists of the resolution of the φ-FEM problem 7 or the resolution of a standard FEM problem (on a conforming mesh) associated with eq. (1).
- The ESTIMATE module consists of the computation of the residual estimator η, or the standard FEM residual estimator (i.e. without the boundary correction term η_ε).
- The MARK module is the Dörfler's marking strategy [14] with parameter $\theta = 0.3$.
- For the REFINE module we use the `refine` routine of the FEniCSx software which (in 2D) adds a new degree of freedom at the midpoint of the marked facets and refine the neighbors cells accordingly. In the φ-FEM case, after each refinement, some cells might end up strictly outside Ω_h. These cells are removed from the mesh for the next iteration since they are not used in the φ-FEM solver. However, by doing so, there is a chance for some parts of Ω to end up outside Ω_h and to be lost forever since no new cell is created outside the existing ones. To prevent this, we start the refinement loop with a box mesh such that $\Omega \subset \cup_{T\in\mathcal{T}_h} T$ and then at each iteration, we use a fine interpolation $\hat{\varphi}_h$ of the levelset function (e.g. in a Lagrange finite element space of degree 2) in order to detect the cells cut by Γ. For each cell $T \in \mathcal{T}_h$ we compute the following detection function:

$$\frac{\sum\limits_{\text{dof in } T} \hat{\varphi}_h(\text{dof})}{\sum\limits_{\text{dof in } T} |\hat{\varphi}_h(\text{dof})|} = \begin{cases} -1 & \text{if } T \subset \{\hat{\varphi}_h < 0\}, \\ 1 & \text{if } T \subset \{\hat{\varphi}_h > 0\}, \\ \alpha & \in (-1,1), \text{ if } T \cap \{\hat{\varphi}_h = 0\} \neq \varnothing. \end{cases} \tag{25}$$

  This allows for more precise detection of the boundary Γ and can help prevent losing parts of Ω during the refinement process. On the left of fig. 1 we can see that a piecewise linear $\hat{\varphi}_h$ fails to detect the corners of the square Ω. However, using a piecewise quadratic $\hat{\varphi}_h$ solves the issue in this case. Note that the use of $\hat{\varphi}_h$ is only for boundary detection; a coarser interpolation is used in the rest of the adaptation modules.

In the following, we will talk about AFEM (resp. Aφ-FEM) when the loop is based on standard FEM (resp. φ-FEM).

6.1 First test case : product of sines

Let us denote by $r_\theta : \mathbb{R}^2 \to \mathbb{R}^2$ the rotation of angle θ, i.e.

$$r_\theta(x, y) = \begin{pmatrix} \cos(\theta) & -\sin(\theta) \\ \sin(\theta) & \cos(\theta) \end{pmatrix} \begin{pmatrix} x \\ y \end{pmatrix}.$$

We consider Ω to be the centred unit square $(-0.5, 0.5)^2$ tilted by an angle of $\theta = -\pi/6$. Given $\varphi^*(x, y) = |x| + |y| - \sqrt{2}/2$, the domain Ω is defined by the levelset

$$\varphi(x, y) = \varphi^* \circ r_{\pi/6-\pi/4}(x, y).$$

Given $f^*(x, y) = 8\pi^2 \sin(2\pi x) \sin(2\pi y)$, the source term is defined by

$$f(x, y) = f^* \circ r_{\pi/6}(x, y),$$

so that the exact solution to eq. (1) is given by

$$u_{\text{exact}}(x, y) := u^* \circ r_{\pi/6}(x, y),$$

where $u^*(x, y) = \sin(2\pi x) \sin(2\pi y)$. In this case, the error will be computed with respect to u_{ref}, an interpolation of u_{exact} in a finer finite element space.

In fig. 2 are shown the initial meshes and meshes after 10 adaptive refinement iterations of AFEM and Aφ-FEM, respectively. The solutions for FEM and φ-FEM after 10 iterations of the adaptive refinement loop are shown on fig. 3.

On fig. 4, we compare the convergence curves of the residual estimator η and the exact error $|u_{\text{ref}} - u_h|_{H^1(\Omega)}$ for both uniform and adaptive mesh refinement with φ-FEM. All the curves have an optimal slope, which indicates that η is able to correctly distribute the refinement across the mesh. Given the regularity of the exact solution of this test case, uniform and adaptive refinement are expected to have identical convergence slopes.

On the top of fig. 5, we compare the convergence of $|u_{\text{ref}} - u_h|_{H^1(\Omega)}$ and η for FEM and φ-FEM. As we can see, the slopes are optimal for both φ-FEM and FEM. In this case φ-FEM has a slightly smaller exact error compared to FEM.

On the bottom of fig. 5, we show the convergence of η and its contributions η_r, η_J and η_ε. Due to the simple geometry of Ω, the contribution of the boundary correction η_ε is much smaller than η_r and η_J. Essentially, the boundary approximation error is concentrated at the corners of the domain. This explains why the estimators values for FEM and φ-FEM are very close from each other.

6.2 Second test case : L-shaped domain

In this test case, the domain Ω is a tilted and shifted L-shaped domain as shown on fig. 6, where the corresponding levelset function is represented. The shift is chosen such that the reentrant corner vertex of Ω does not fall exactly on a vertex of the initial φ-FEM mesh. The levelset φ is obtained by taking successive maxima and minima between linear functions. The source term f is constant equal to 1. In this case, since no analytical solution is available, the error is computed with respect to u_{ref} given as a standard finite element solution computed on an overrefined conforming mesh.

On fig. 7, we show the initial meshes, the meshes after 10 iterations and the final meshes of AFEM and Aφ-FEM, respectively. As we can notice, the local refinement occurs in the expected reentrant corner region of the domain for both AFEM and Aφ-FEM. This, for Aφ-FEM, is supported by fig. 8, on which we can see the local contributions of the estimators compared to the local contributions of the exact error $|u_{\text{ref}} - u_h|_{H^1(\Omega)}$. We remark that the estimator is efficient at spotting the region of highest discretization error. In fig. 9, we provide the contribution of each

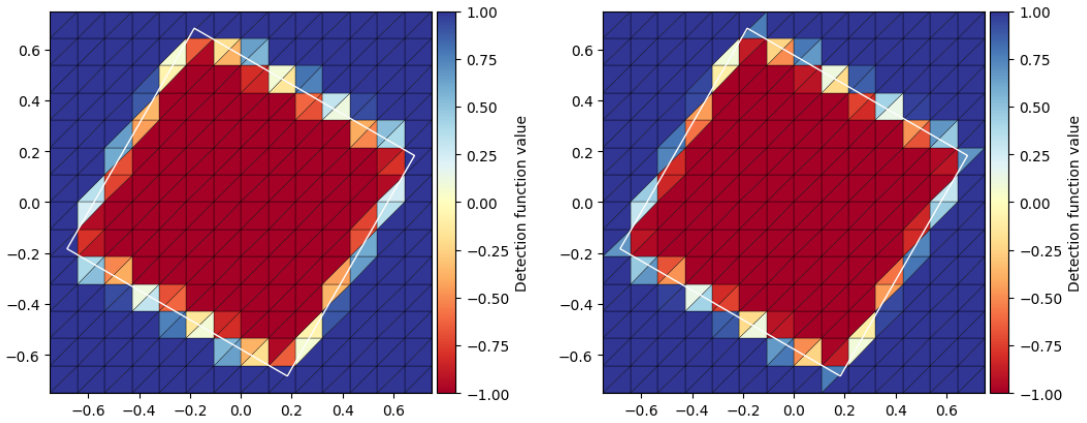

Figure 1: **Product of sines:** The detection function (eq. (25)) on the initial box mesh, for $\hat{\varphi}_h$ piecewise linear on the left and for $\hat{\varphi}_h$ piecewise quadratic on the right. The white square represents the exact boundary Γ.

term of the estimator. We can see that the boundary correction term detect the singularity of the geometry localized on the corners.

On fig. 10, we compare the convergence curves for uniform refinement and adaptive refinement with φ-FEM. As expected for this test case, the error's convergence slopes (left) are suboptimal for uniform refinement, and the optimality is recovered by adaptive refinement. This suggests that Aφ-FEM can properly adapt meshes to the local features of the solution. In the right graph, we represent the different parts of the estimator. Again, we remark that the boundary correction term η_ε is smaller than the others. This is due to the simplicity of the geometry of Ω. In fig. 10, we can see that the convergence slopes for AFEM, and Aφ-FEM in the case of adaptive refinement are very similar. On fig. 11, we show the efficiency indices of η for both FEM and φ-FEM and for both uniform (left) and adaptive (right) refinement. As we can see, the efficiency indices of the FEM and φ-FEM estimators are close.

6.3 Third test case: Flower shaped domain test case

This test case is taken from [10]. Here, Ω is "flower shaped" with a curved boundary and several reentrant corners, as shown on fig. 12 (left). The source term f is piecewise constant and equals 10 inside the circle (see fig. 12, left) and 0 outside. Let

$$\varphi_0(x, y) = x^2 + y^2 - 4, \tag{26}$$

and

$$\varphi_i(x, y) = (x - x_i)^2 + (y - y_i)^2 - r \quad \forall i = 1, \dots, 9, \tag{27}$$

where for $i = 1, \dots, 9$,

$$\begin{cases} x_i = 2(\cos(\pi/8) + \sin(\pi/8))\cos(i\pi/4) \\ y_i = 2(\cos(\pi/8) + \sin(\pi/8))\sin(i\pi/4) \end{cases}, \quad \text{and} \quad r = 2\sqrt{2}(\cos(\pi/8) + \sin(\pi/8))\sin(\pi/8). \tag{28}$$

The levelset associated with Ω is given by

$$\varphi = \min(\varphi_0, \varphi_1, \dots, \varphi_9). \tag{29}$$

The solution to eq. (7) after 17 Aφ-FEM iterations is shown on fig. 12 (right).

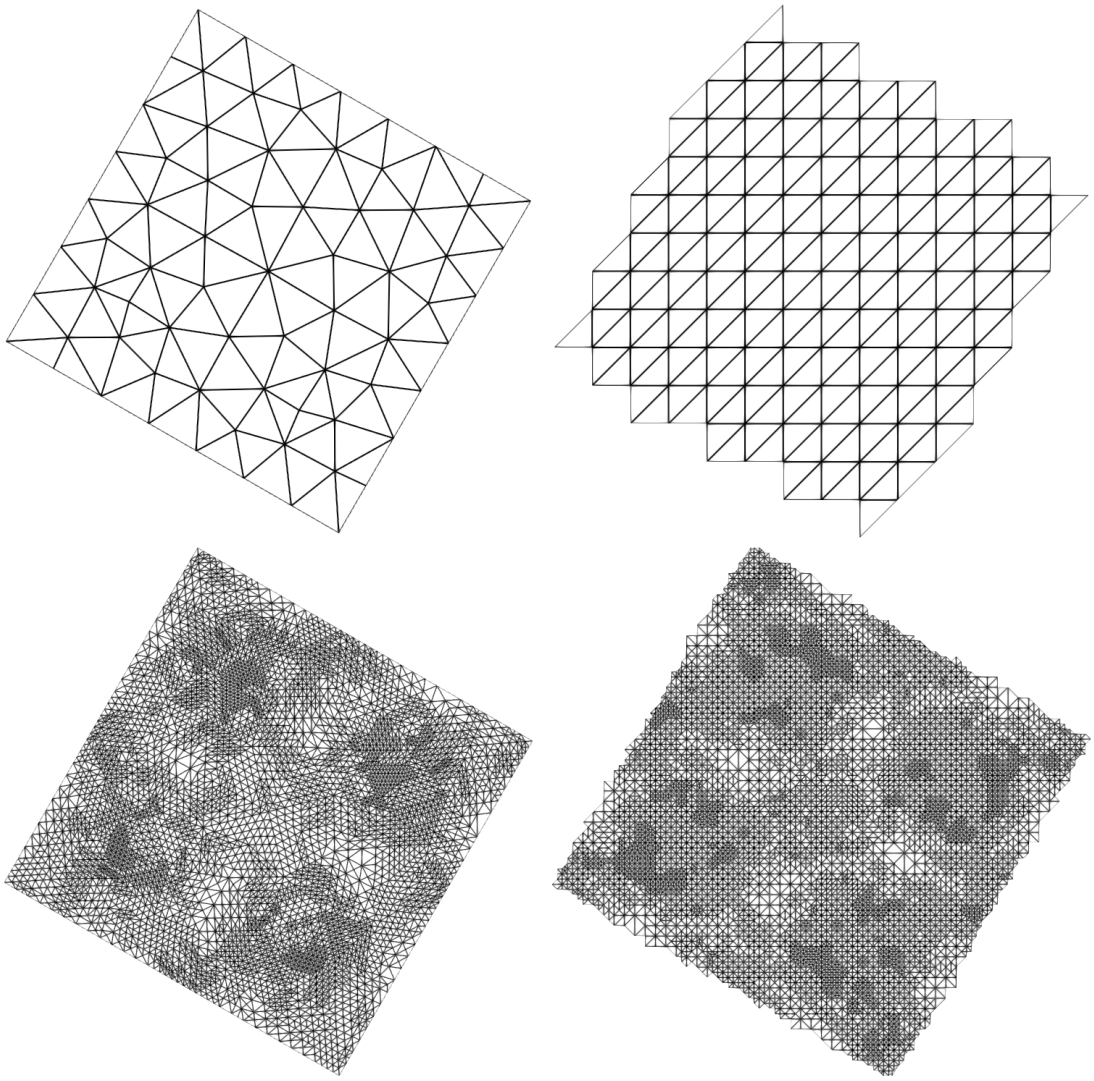

Figure 2: **Product of sines:** On the top row, the initial meshes used for AFEM (left) and Aφ-FEM (right). On the bottom row, the meshes after 10 iterations of AFEM (left) and Aφ-FEM (right).

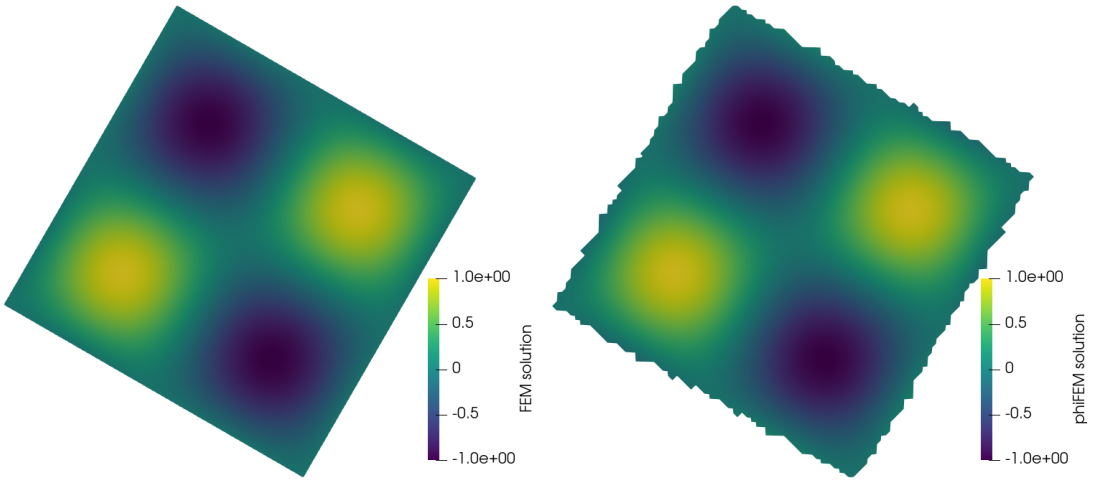

Figure 3: **Product of sines:** The solutions u_h after 10 adaptive refinement steps, AFEM on the left, Aφ-FEM on the right.

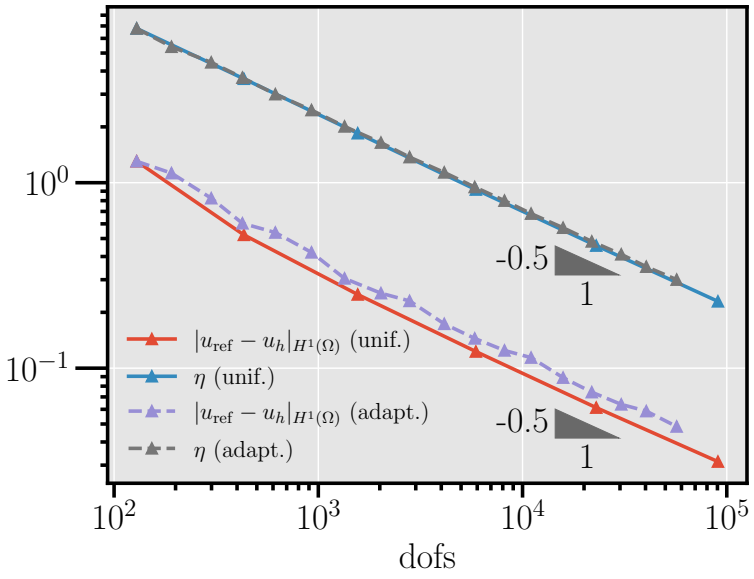

Figure 4: **Product of sines:** Comparison of the convergence curves of the estimator η and the exact error in H^1 semi-norm for uniform and adaptive mesh refinement for φ-FEM.

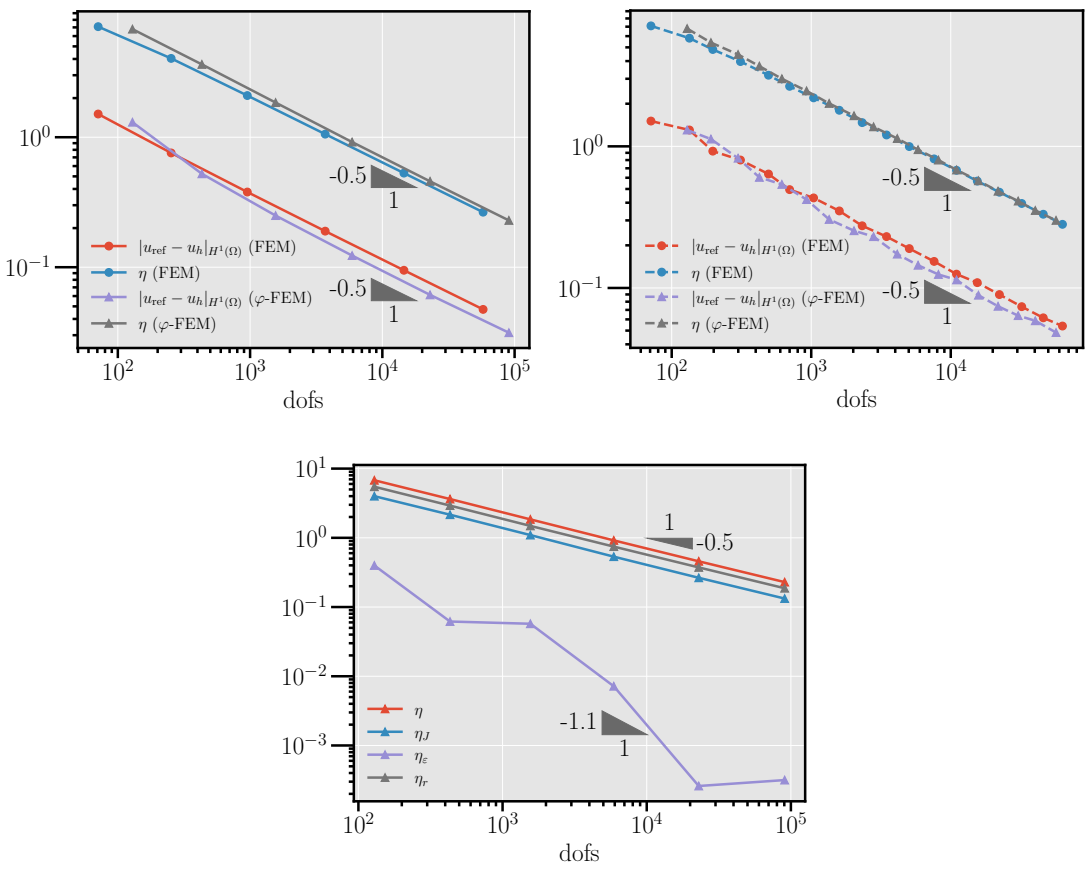

Figure 5: **Product of sines:** On the top, the comparison of the convergence curves of the estimators for FEM and φ-FEM. Uniform refinement on the left, adaptive refinement on the right. On the bottom, the comparison of the convergence curves of the estimator η and its contributions η_r, η_J and η_ε.

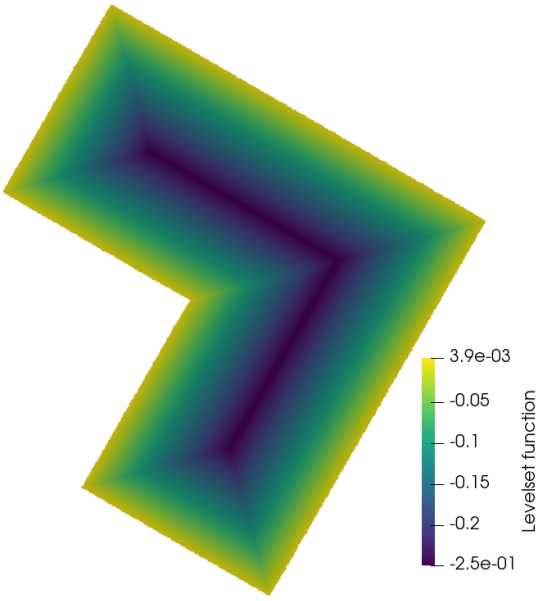

Figure 6: **L-shaped domain:** The levelset φ defining the L-shaped domain Ω.

On fig. 13, we see the meshes at different Aφ-FEM refinement steps. As expected, most of the refinement occurs on the right part of the domain, where the solution shows the most variations. We also notice refinement near the reentrant corners, where the gradient of the solution is singular. Remark also that the Aφ-FEM algorithm can fit the shape of the domain Ω pretty well, avoiding useless mesh data being stored.

The graph on the top of fig. 14 shows the convergence slopes of the estimator during uniform refinement and Aφ-FEM loops. The estimators show expected convergence slopes, with optimality recovered thanks to adaptive refinement for η. On the bottom left of fig. 14 we detail the convergence of the contributions η_r, η_J and η_ε for uniform refinement. As we can see, the boundary correction term becomes constant after few iterations. This suggests that uniform refinement is unable to fit the geometry of Ω. On the bottom right of fig. 14, we notice that, as for the previous cases the boundary correction term is much smaller than the other contributions.

7 Acknowledgment

This work was supported by the Agence Nationale de la Recherche, Project PhiFEM, under grant ANR-22- CE46-0003-01.

References

[1] Mark Ainsworth and J Tinsley Oden. *A Posteriori Error Estimation in Finite Element Analysis*. John Wiley & Sons, Inc., Hoboken, NJ, USA, August 2000.

[2] Mark Ainsworth and Richard Rankin. Computable error bounds for finite element approximation on nonpolygonal domains. *IMA Journal of Numerical Analysis*, 37(2):604–645, April 2017.

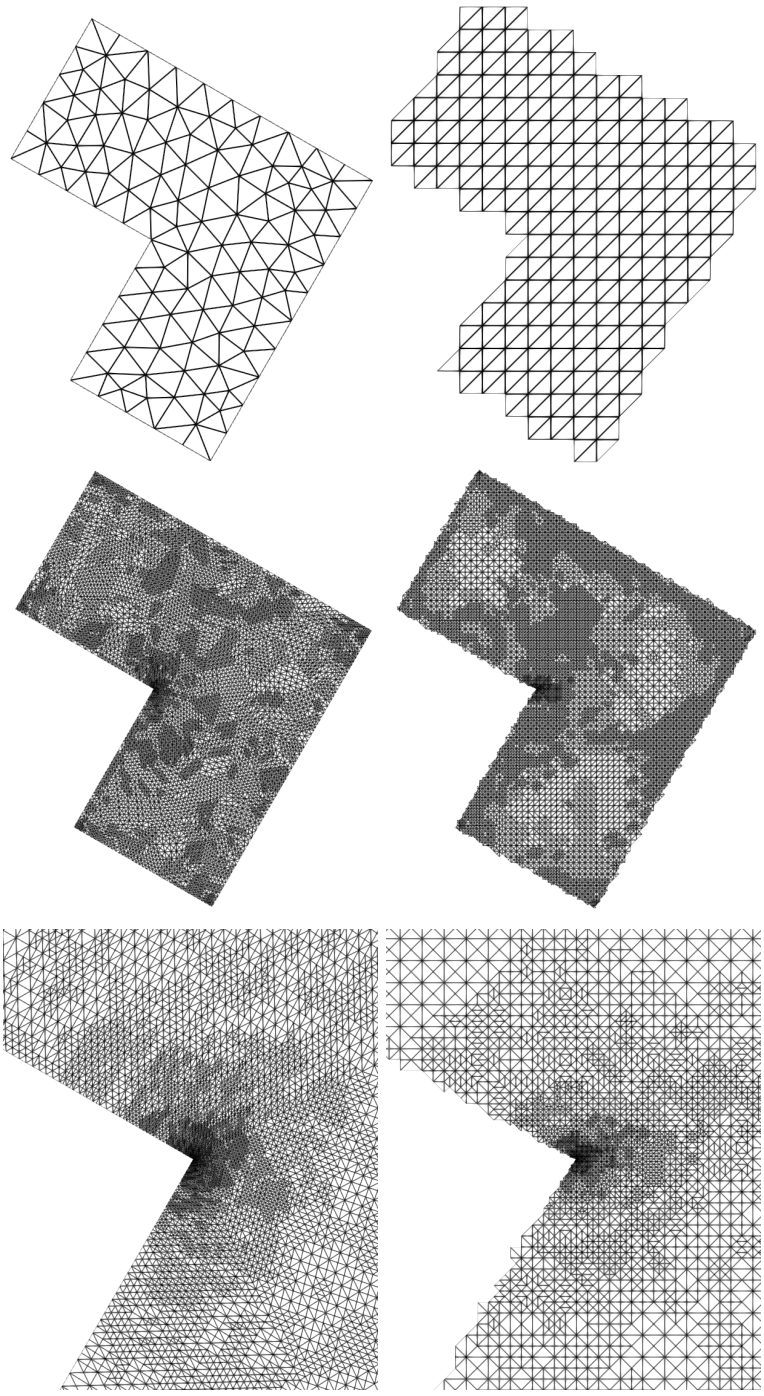

Figure 7: **L-shaped domain:** On the top row,the initial meshes used for AFEM (left) and Aφ-FEM (right). On the middle row, the meshes after 10 iterations of AFEM (left) and Aφ-FEM (right) steered by η. On the bottom row, zooms on the reentrant corner of the meshes after 19 iterations of AFEM (left) and Aφ-FEM (right).

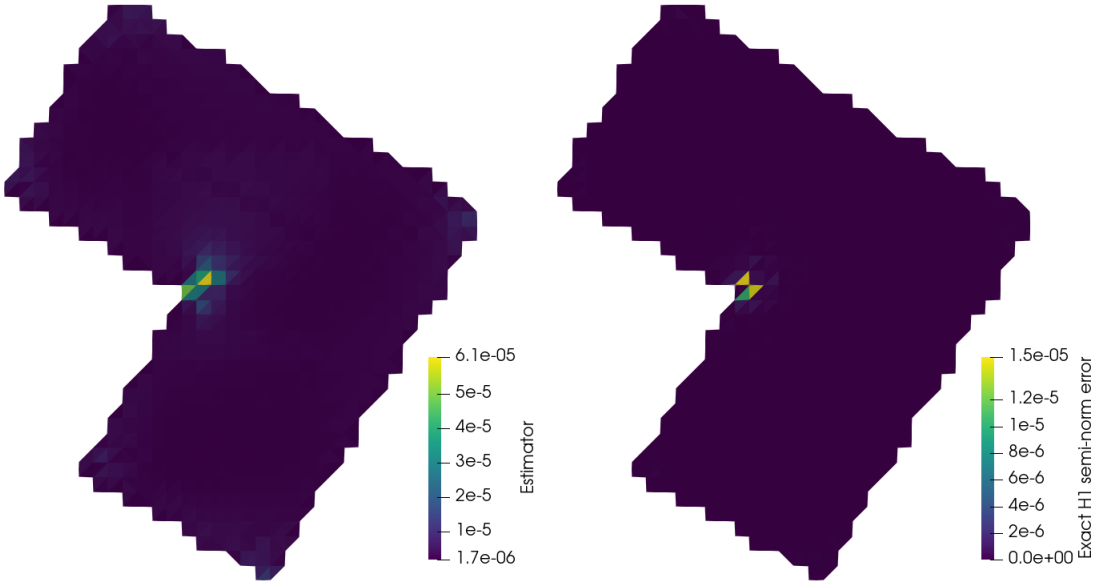

Figure 8: **L-shaped domain:** The local contributions of η (left) and of the exact H^1 semi-norm error (right) after 3 Aφ-FEM iterations.

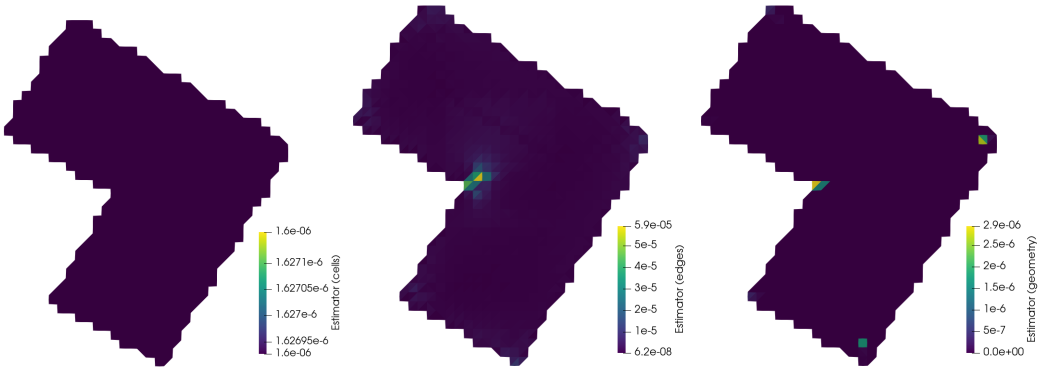

Figure 9: **L-shaped domain:** From left to right, the local contributions of η_{cell}, η_{facets} and η_ε for Aφ-FEM.

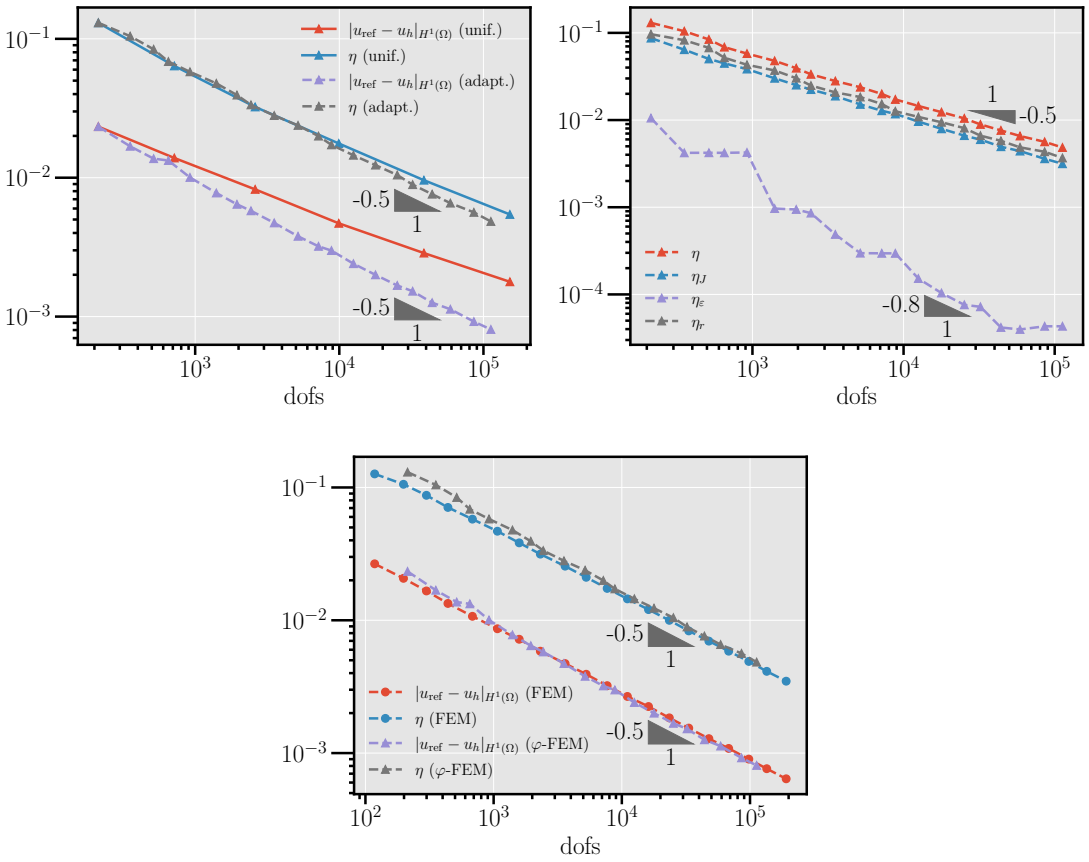

Figure 10: **L-shaped domain:** On the top left, the comparison of the convergence curves of η and the exact H^1 semi-norm error for uniform and adaptive mesh refinement for φ-FEM. On the top right, the comparison of the convergence curves of the estimator η and its contributions η_r, η_J and η_ε. On the bottom, comparison of the adaptive mesh refinement for φ-FEM and FEM.

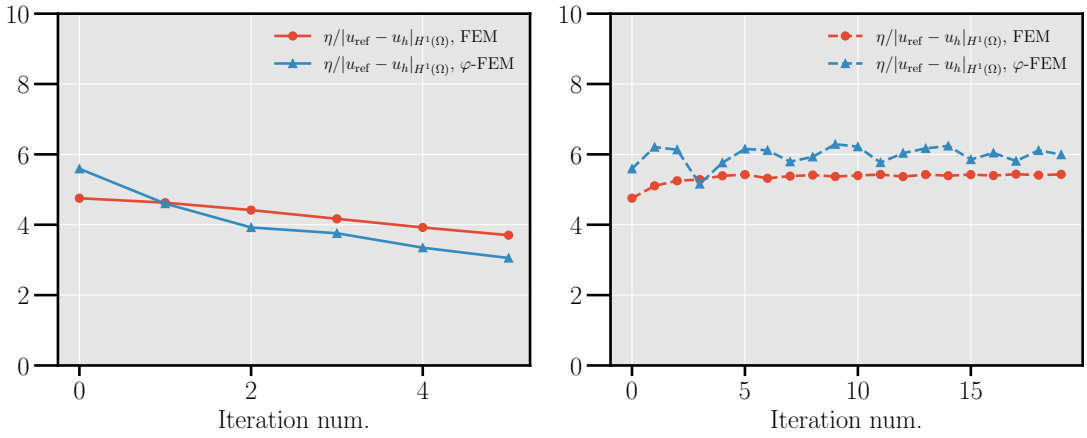

Figure 11: **L-shaped domain:** Comparisons of the efficiency indices for FEM and φ-FEM. On the left, for uniform refinement. On the right, for adaptive refinement.

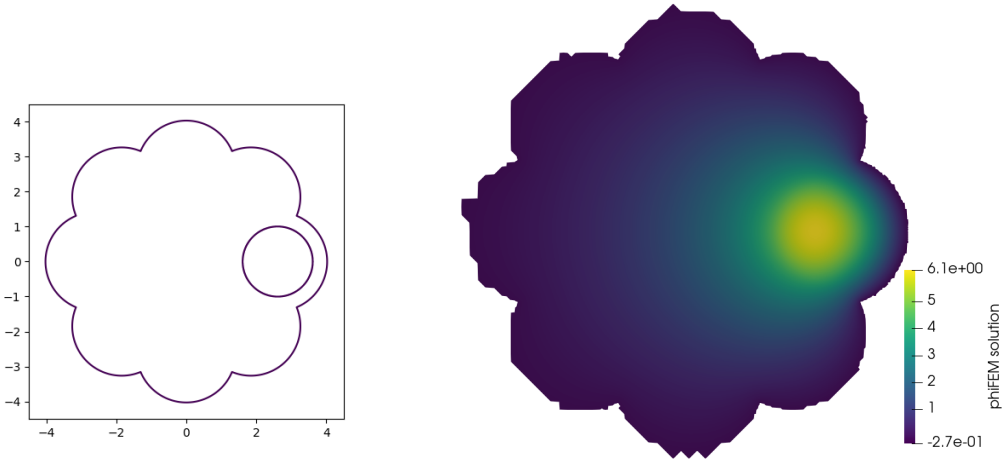

Figure 12: **Flower shaped domain:** On the left, the domain Ω. The circle on the right is the boundary of the support of the source term f. On the right, the φ-FEM solution after 17 Aφ-FEM iterations.

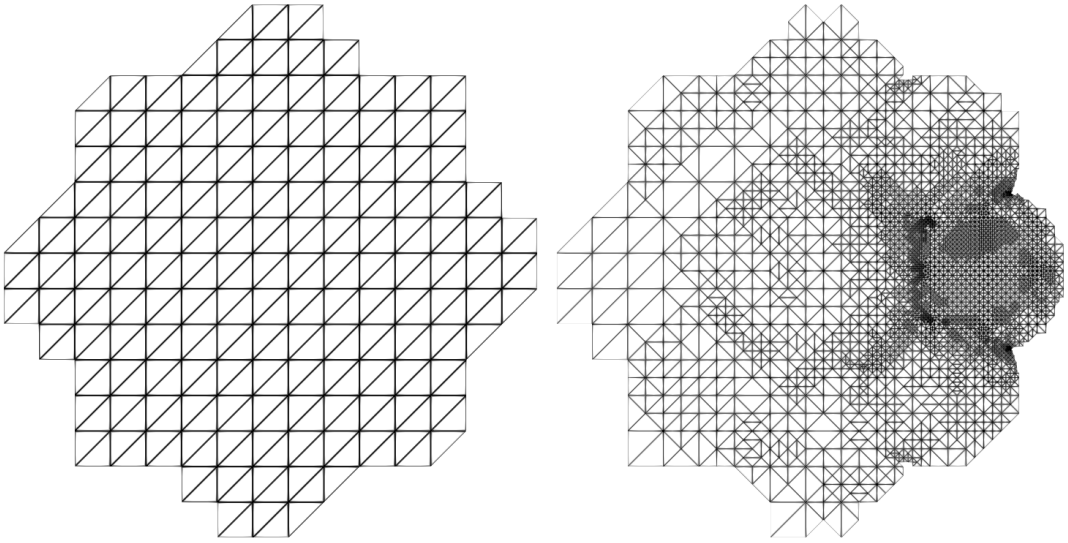

Figure 13: **Flower shaped domain:** On the left the initial mesh and on the right the mesh after 10 Aφ-FEM iterations.

[3] Najwa Alshehri, Daniele Boffi, and Lucia Gastaldi. A posteriori error estimator for elliptic interface problems in the fictitious formulation. *arXiv preprint arXiv:2407.00786*, 2024.

[4] Igor A. Baratta, Joseph P. Dean, Jørgen S. Dokken, Michal Habera, Jack S. Hale, Chris N. Richardson, Marie E. Rognes, Matthew W. Scroggs, Nathan Sime, and Garth N. Wells. DOLFINx: the next generation FEniCS problem solving environment. *preprint*, 2023.

[5] Annalisa Buffa, Ondine Chanon, Denise Grappein, Rafael Vázquez, and Martin Vohralík. An equilibrated flux a posteriori error estimator for defeaturing problems. *SIAM Journal on Numerical Analysis*, 62(6):2439–2458, 2024.

[6] E. Burman. Ghost penalty. *C. R. Math. Acad. Sci. Paris*, 348(21-22):1217–1220, 2010.

[7] E. Burman and P. Hansbo. Fictitious domain finite element methods using cut elements: I. A stabilized Lagrange multiplier method. *Computer Methods in Applied Mechanics and Engineering*, 199(41):2680–2686, 2010.

[8] E. Burman and P. Hansbo. Fictitious domain finite element methods using cut elements: II. A stabilized Nitsche method. *Applied Numerical Mathematics*, 62(4):328–341, 2012.

[9] E. Burman and P. Hansbo. Fictitious domain methods using cut elements: Iii. a stabilized nitsche method for stokes problem. *ESAIM: Mathematical Modelling and Numerical Analysis*, 48(3):859–874, 2014.

[10] Erik Burman, Cuiyu He, and Mats G Larson. A posteriori error estimates with boundary correction for a cut finite element method. *IMA Journal of Numerical Analysis*, 42(1):333–362, January 2022.

[11] Stéphane Cotin, Michel Duprez, Vanessa Lleras, Alexei Lozinski, and Killian Vuillemot. ϕ-fem: An efficient simulation tool using simple meshes for problems in structure mechanics and heat transfer. *Partition of Unity Methods*, pages 191–216, 2023.

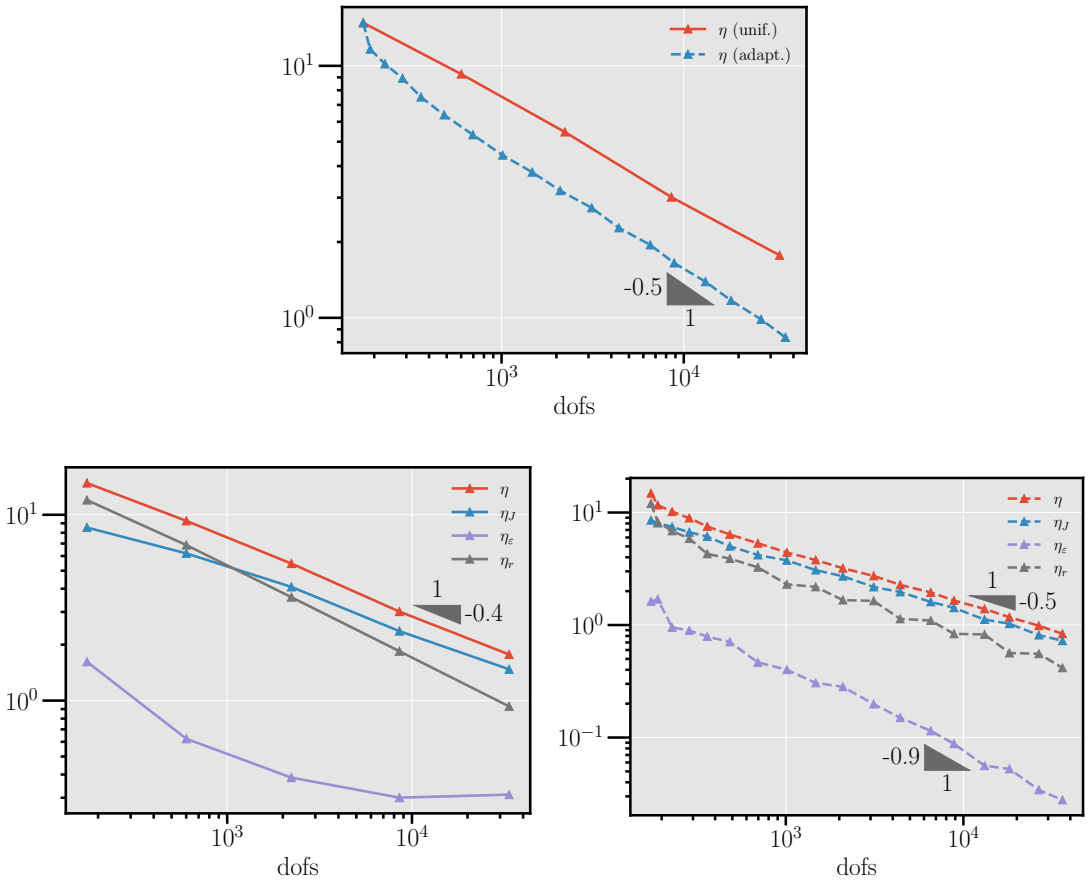

Figure 14: **Flower shaped domain (φ-FEM):** On the top, the comparison of the convergence curves of η for uniform and adaptive mesh refinement. On the bottom, the comparison of the local contributions of η_{cell}, η_{facets} and η_{geom} for uniform mesh refinement (left) and adaptive mesh refinement (right).

[12] Paolo Di Stolfo and Andreas Schröder. Reliable residual-based error estimation for the finite cell method. *Journal of Scientific Computing*, 87(12), February 2021.

[13] W. Dörfler and M. Rumpf. An Adaptive Strategy for Elliptic Problems Including a Posteriori Controlled Boundary Approximation. *Mathematics of Computation*, 67(224):1361–1382, 1998.

[14] Willy Dörfler. A convergent adaptive algorithm for poisson's equation. *SIAM Journal on Numerical Analysis*, 33(3):1106–1124, 1996.

[15] Michel Duprez, Vanessa Lleras, and Alexei Lozinski. A new ϕ-fem approach for problems with natural boundary conditions. *Numerical Methods for Partial Differential Equations*, 39(1):281–303, 2023.

[16] Michel Duprez, Vanessa Lleras, and Alexei Lozinski. ϕ-fem: an optimally convergent and easily implementable immersed boundary method for particulate flows and stokes equations. *ESAIM: Mathematical Modelling and Numerical Analysis*, 57(3):1111–1142, 2023.

[17] Michel Duprez, Vanessa Lleras, Alexei Lozinski, and Killian Vuillemot. ϕ-fem for the heat equation: optimal convergence on unfitted meshes in space. *Comptes Rendus. Mathématique*, 361(G11):1699–1710, 2023.

[18] Michel Duprez and Alexei Lozinski. ϕ-FEM: A Finite Element Method on Domains Defined by Level-Sets. *SIAM J. Numer. Anal.*, 58(2):1008–1028, January 2020.

[19] Alexandre Ern and Jean-Luc Guermond. *Theory and practice of finite elements*, volume 159. Springer, 2004.

[20] Vivette Girault and Roland Glowinski. Error analysis of a fictitious domain method applied to a dirichlet problem. *Japan Journal of Industrial and Applied Mathematics*, 12:487–514, 1995.

[21] R. Glowinski, T. Pan, and J. Periaux. A fictitious domain method for Dirichlet problem and applications. *Computer Methods in Applied Mechanics and Engineering*, 111(3-4):283–303, 1994.

[22] Cuiyu He, Shun Zhang, and Xu Zhang. Error analysis of *p*etrov-*g*alerkin immersed finite element methods. *Computer Methods in Applied Mechanics and Engineering*, 404:115744, 2023.

[23] Cuiyu He and Xu Zhang. Residual-based a posteriori error estimation for immersed finite element methods. *Journal of Scientific Computing*, 81(3):2051–2079, nov 2019.

[24] A. Main and G. Scovazzi. The shifted boundary method for embedded domain computations. Part I: Poisson and Stokes problems. *J. Comput. Phys.*, 372:972–995, 2018.

[25] Khamron Mekchay and Ricardo H Nochetto. Convergence of adaptive finite element methods for general second order linear elliptic pdes. *SIAM Journal on Numerical Analysis*, 43(5):1803–1827, 2005.

[26] R. Mittal and G. Iaccarino. Immersed boundary methods. *Annu. Rev. Fluid Mech.*, 37:239–261, 2005.

[27] Jamshid Parvizian, Alexander Düster, and Ernst Rank. Finite cell method: h-and p-extension for embedded domain problems in solid mechanics. *Computational Mechanics*, 41(1):121–133, 2007.

[28] Elias M Stein. *Singular integrals and differentiability properties of functions*. Princeton university press, 1970.

[29] Rüdiger Verfürth. *A posteriori error estimation techniques for finite element methods*. OUP Oxford, 2013.